LAWRENCE
LIVERMORE
NATIONAL
LABORATORY

LLNL-JRNL-513474

Sub-100 ps laser-driven dynamic compression of solid deuterium with a ~40 (mu)J laser pulse

M. Armstrong, J. Crowhurst, S. Bastea, J. Zaug, A. Goncharov

November 11, 2011

Applied Physics Letters

Disclaimer

Sub-100 ps laser-driven dynamic compression of solid deuterium with a ~40 μJ laser pulse

Michael R. Armstrong*, Jonathan C. Crowhurst, Sorin Bastea, and Joseph M. Zaug

Physical and Life Sciences Directorate, Lawrence Livermore National Laboratory, Livermore, California 94550, USA

Alexander F. Goncharov

Geophysical Laboratory, Carnegie Institute of Washington, Washington, DC 20015, USA

*email: armstrong30@llnl.gov

Abstract

We dynamically compress solid deuterium over <100 ps from initial pressures of 22 GPa to 55 GPa, to final pressures as high as 71 GPa, with <40 μJ of pulse energy. At 25 GPa initial pressure, we measure compression wave speeds consistent with quasi-isentropic compression and a 24% increase in density. The laser drive energy per unit density change is 10^9 times smaller than it is for recent longer (~30 ns) time scale compression experiments. This suggests that, for a given final density, dynamic compression of hydrogen might be achieved using orders of magnitude lower laser energy than currently used.

Materials at high density are central to fundamental physics[1–6,] and planetary science[7]. Hydrogen at high density is of great interest for fundamental properties[8–10] and inertial confinement fusion[5]. Generally, dynamic methods employing compression waves are required to obtain the highest compressions, and facility-sized instruments have been constructed to perform large scale laser-driven dynamic compression experiments[5,6,11–13].

"Slow"[14] compression[4,13,15] is essential to obtain high density hydrogen[4], since shockwave (fast) compression cannot achieve high density[6,16] due to the production of dissipative heat.[6,15] It was recently shown conceptually that the energy required to dynamically compress a sample varies as the third power of the compression time[17], ie. a reduction in the compression time by a factor of 10 reduces the required compression energy by a factor of 1000. In conventional laser driven dynamic compression, the compression time scale typically ranges from 10-100 ns.[11,13]

Thus, for materials which equilibrate on a picosecond time scale, the drive energy for dynamic compression experiments can be orders of magnitude smaller than currently used. For example, recently Fe (which does not equilibrate rapidly) was ramp compressed to ~1.67x initial density over <30 ns using 285 kJ of pulse energy[13]. Here, we quasi-isenstropically compress solid deuterium (at an initial pressure of 24 GPa) to ~1.24x initial density over <100 ps using <40 μJ of pulse energy. The laser drive energy per unit density change in these experiments is ~10^9 times smaller than the longer time scale experiments. Even accounting for the relatively small difference between the bulk

modulus of Fe (170 GPa) and deuterium (70 GPa at 24 GPa pressure[18]), this result suggests that, for a given final density, because it equilibrates rapidly hydrogen might be compressed using orders of magnitude lower drive energy than used in longer time scale experiments. This is a substantial experimental advantage, enabling relatively high throughput[13,19], and more extreme conditions for a given laser drive energy.

These results apply broadly to dynamically compressed hydrogen outside the DAC. Usually, hydrogen has been dynamically compressed from a cryogenic liquid or solid at low pressure.[20] Although we compress solid deuterium in a DAC, it is very likely that cryogenic liquid deuterium equilibrates on a faster time scale than the solid deuterium in our experiments. Boehly et al.[20], in shock compression experiments of cryogenic liquid deuterium which reach a final pressure of 2500 GPa, measure a single shock rise time (which is comparable to the equilibration time) of less than 22 ps. Thus, compression of cryogenic liquid deuterium to extreme density is likely possible with a compression time of much less than 1 ns.

Also, at least one solid, Al, is known to exhibit stiff behavior under fast compression, in contrast to our results for solid deuterium.[15] Here we apply ultrafast laser compression and diagnostic methods[11,19,21–27] to demonstrate quasi-isentropic compression of solid deuterium in less than 100 ps, at least an order of magnitude faster than conventional quasi-isentropic dynamic compression[6,12,13,15,20].

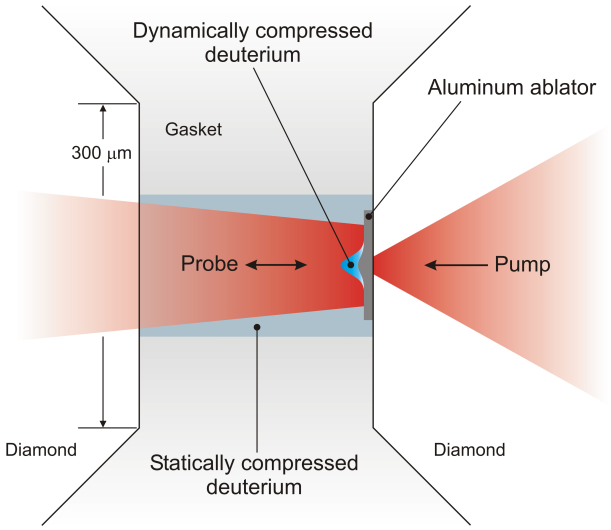

Figure 1: An experimental schematic, where the horizontal dimension of the sample cavity has been expanded by a factor of ~30.

We identify quasi-isentropic compression via a measurement of the compression wave speed via an oscillatory interferometric optical reflectivity signal[19,21,28] (see below), where the period of oscillation decreases monotonically with increasing wave speed. For compression over a sub-100 ps time scale, the period of the observed oscillations must be sufficiently short (consistent with a sufficiently large wave speed) to observe a period of oscillation in the signal over the compression time. In part to satisfy this requirement, we obtain sufficiently fast wave speeds by precompressing the deuterium (D_2) sample in a diamond anvil cell (DAC). After the initial static precompression, we dynamically compress the sample from initial pressures ranging from 22 GPa to 55 GPa at room temperature to final stresses as high as 71 GPa, over time scales of tens of picoseconds, using ultrafast laser driven dynamic compression as described in refs. 21 and 19.

A schematic drawing of the experiment is shown in Fig. 1. A ~1 micron aluminum

ablation layer partially coats one tip of one diamond of the DAC. The initial pressure in the DAC was determined using ruby fluorescence[29]. A laser pump pulse was used to drive a compression wave into the Al ablation layer, which, after transiting the ablation layer, dynamically compressed the deuterium sample. The pump pulse energy measured before entering the DAC ranged between 30-40 μJ and the pump spot size at the ablator was ~20 μm FWHM in diameter. The pump pulse temporal profile was a clipped gaussian, with an initial fast (~5 ps) rise and ~100 ps duration, similar to previous work[19,21,22,26,30]. The peak intensity of the pump was approximately 10^{11} W/cm^2. The radius of curvature of the of the compression front is much larger (>200x) than the distance over which the waves propagate, so the flow is approximately 1D[17]. These experiments result in localized damage at the pump spot – each dataset was obtained in single shot, but more than one shot could be obtained from a single DAC load.

The probe comprised a pair of low energy (~ 5 μJ) pulses with the same temporal characteristics as the pump, delayed with respect to each other by 5 ps, with a spot diameter on the sample of greater than 200 μm. The probe pulses are Doppler shifted upon reflection from the moving compression wave and D_2/Al (piston) interface[19,21,22] (which is directly analogous to picosecond acoustic spectroscopy[28]). The observable is an optical phase shift between the two probe pulses resulting from these Doppler shifted reflections, as a function of time. Two examples of the raw data are shown in Fig. 2. Time resolution in these experiments is obtained by spectrally resolving chirped probe pulses, where the wavelength of the probe sweeps over its bandwidth as a function of time (i.e.

early times in the pulse are red, late times are blue). This method is commonly employed to obtain a full window of data in a single shot for ultrafast shock wave experiments[19,21,22,26]. Both pump and probe have an intensity bandwidth of ~25 nm full width at half maximum. Data is obtained over a spatial 1D cut through the pump profile and the time traces are obtained at the center of the pump profile[19,21,26]. Full details of the experimental setup are given in refs. 21 and 19.

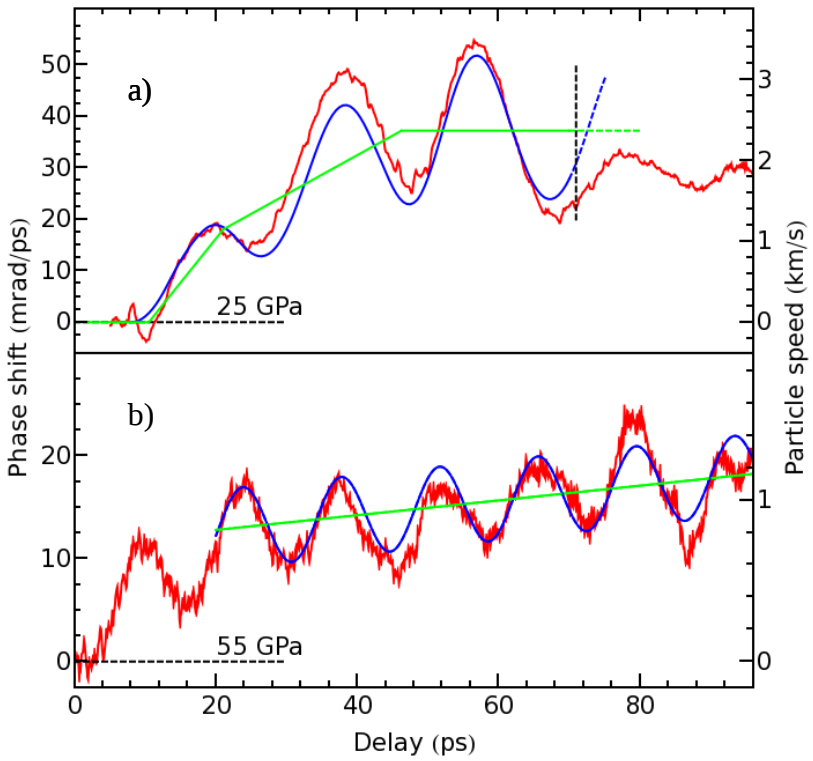

Figure 2: a) Data from dynamically compressed deuterium from an initial pressure of 25 GPa (red), a fit to the data (blue) assuming a quasi-isentropic compression model, and the particle speed at the piston corresponding to the fit (green). The blue and red curves correspond to the left axis and the green curve corresponds to both the left and right axes (see the main text). The dashed blue and green traces show the signal given by the model where the data deviates from the model, and the dashed vertical black line shows the first point of convergence of isobars implied by the model (see below in the main text). Shock formation (and deviation of the signal from the model) would occur just before isobars converge. For these data, compression occurs over ~35 ps and the signal deviates from the fit ~70 ps after the compression wave arrives in the D_2. b) Dynamic compression data from an initial pressure of 55 GPa, resulting in an elastic shock wave.

In general, the data is the sum of two contributions: a monotonic non-oscillatory part (the offset) which is approximated in Fig. 2 by green traces, and a quasi-sinusoidal oscillation centered vertically at the offset. When the Gladstone-Dale approximation[31] is valid (as it is here)[32], the particle speed at the piston is given by the offset via $particle\ speed = offset * \lambda / (4\pi)$, as shown on the right side axes of the plots. The

compression wave front and the piston interface form an etalon with an optical pathlength that increases with time as the compression front outruns the piston. A single cycle of oscillation corresponds to a half wavelength of optical pathlength between the piston and the compression wave front, enabling a measurement of the compression wave speed.

There are two types of dynamic response that can in principle occur upon fast, longitudinal, high strain compression of a soft solid.[33,34] Rapid compression (i.e. with a rate comparable to or larger than the relaxation rate) of the sample generates a large longitudinal elastic compression wave near the piston interface, followed after some relaxation time by plastic deformation[30,35]. Compression at a rate slower than the relaxation rate generates a quasi-isentropic compression wave which travels at the wave speed given by the bulk modulus (analogous to the wave speed in a material without shear strength, such as a liquid)[36]. Critically, longitudinal elastic waves speeds in deuterium are more than 25% faster than bulk waves[18] at the pressures of our experiment. So, longitudinal elastic waves are readily distinguishable from bulk compression waves via characterization of the wave speed. For compression that is faster than relaxation, unrelaxed elastic stress in the sample near the piston is comparable to the peak stress applied to the material[30], i.e. large. Thus, for a solid, a compression wave with a bulk wave speed near the piston interface (where these experiments are performed) indicates that the equilibration rate is larger than the compression rate, i.e. quasi-isentropic compression.

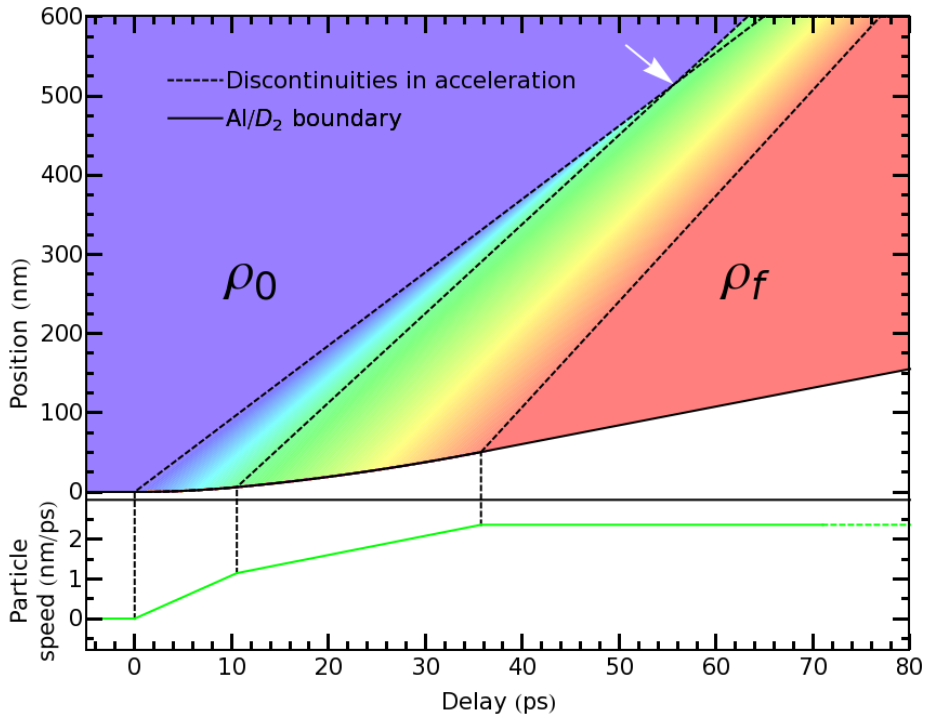

Figure 3: (top) The flow model corresponding to the fit in Fig. 2a (shown as a blue line in Fig. 2a) and (bottom) the piston speed assumed by the model (shown as a green line in Fig. 2a also). The position of the piston surface is shown as a solid line in the top plot. Each isobar (i.e. constant color) corresponds to a pressure-density state along the thermodynamic isentrope. Dashed lines correspond to discontinuities in the acceleration (upper plot), at kinks in the approximate piecewise linear particle speed profile used for the fit, indicated by vertical dashed lines. The first convergence of isobars is labeled by a white arrow. This occurs at the latest time at which a shock wave (comprising the converging isobars) would form.

To characterize the wave speed distribution of compression waves in our experiment, we fit the data to the simulated signal given by a conventional quasi-isentropic compression model of the compression wave[36]. This model assumes the sample behaves as a fluid without shear strength, i.e. the wave speed is given by the bulk modulus of the sample, rather than a longitudinal elastic modulus (e.g. Young's modulus). An example of this

model (corresponding to the fit in Fig. 2a) is shown in Fig. 3. The thermodynamic isentrope, in combination with a particle speed boundary condition at the piston interface completely specifies the fluid flow[36]. In particular, the wave speed of a given pressure-density state (i.e. the slope of an isobar in Fig. 3) is the sum of the local sound and particle speeds, where the local sound speed is given by $\sqrt{(\partial P/\partial \rho)_S}$, and the particle speed along an isobar is set by the piston speed boundary condition. We use "quasi-isentropic" to refer to compression by a wave whose speed is derived from the bulk sound speed of a material along the thermodynamic isentrope, consistent with the conventional definition of the speed of sound in a material without strength given above. The pressure-density for a given particle speed is derived from well-known expressions in ref. 36. To derive the optical response, we use the Gladstone-Dale relationship[31] to obtain the index of refraction from the density given by the fluid flow model, and use only first order reflections from the compression wave front to determine the simulated signal[21].

We calculated the isentrope from 24 GPa initial pressure using variational methods[37] calibrated by measured sound speeds[18]. This calculated isentrope gives bulk sound speeds to within 1% of aggregate bulk speeds in experimental sound speed data (which extend to 24 GPa)[18]. To model the signal for fits, we assume the slope of the calculated isentrope (in wave speed vs. particle speed space, where the isentrope is well approximated by a linear function) and use the bulk sound speed at the initial pressure as a fitting parameter. The particle speed boundary condition comprises the remaining fitting parameters, and is

approximated by a piecewise linear function (e.g., green traces in Fig. 2a), a form which has been used to analyze previous experimental data from Al[11,38–40].

The particle speed boundary condition used in the fit must be well-centered vertically on the oscillations in the signal (see, for example Fig. 2a), which strongly constrains the fit. As shown in Fig. 2a and further raw data (shown in the supplemental information), the fits match the data well. The fit parameters are shown in Table I of the supplemental information.

For quasi-isentropic compression, the wave speed of the ramp varies from the bulk sound speed at the initial pressure (and zero initial particle speed) up to the final pressure and peak wave speed (at the final particle speed and pressure-density). Fig. 4 shows the peak wave speed vs. peak pressure given by fits to the deuterium data of Fig. 2a and qualitatively similar data shown (along with a discussion of the error) in the supplemental information. These data are consistent with wave speeds corresponding to quasi-isentropic compression, rather than longitudinal elastic compression and indicate that, from an initial pressure of 25 GPa, we observe quasi-isentropic dynamic compression of solid deuterium to a final pressure as high as 46 GPa in less than 100 ps.

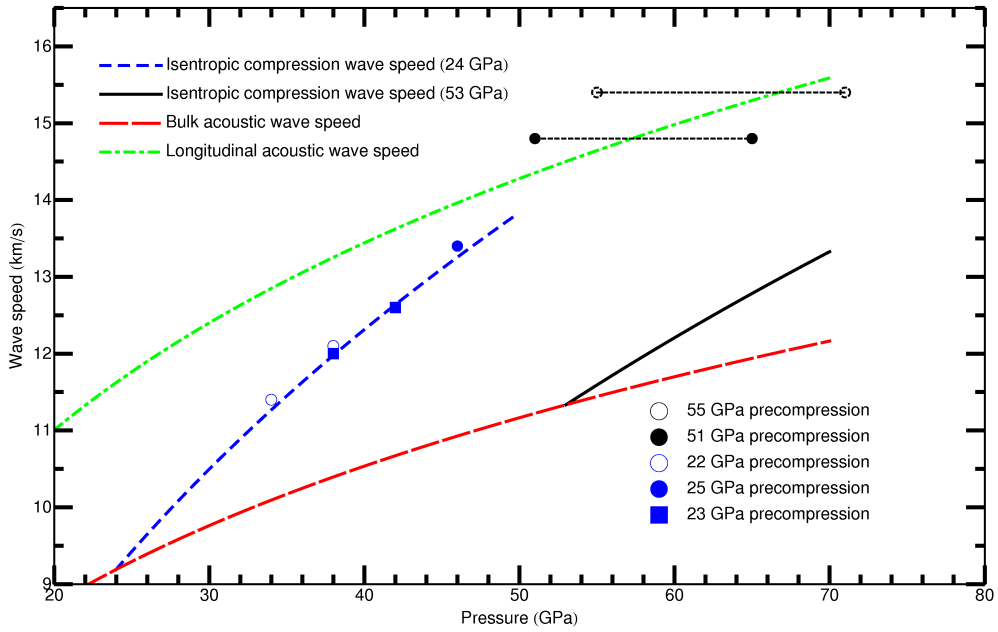

Figure 4: Peak isentropic compression wave speeds (v_m, see Table 1 of the supplemental information) vs peak pressures (P_f) from fits to data (blue points), where each point corresponds to a single shot experiment. Elastic shock wave speeds (u_s, see Table 2 of the supplemental information) in samples at >50 GPa initial precompression are shown in black, where the pressure range (shown as a black dashed line) varies from the initial pressure (P_0) to the final shocked stress (P_f). ~24 GPa and ~53 GPa experimental data may be compared, respectively, to calculated isentropic compression wave speeds vs. pressure for 24 GPa initial pressure (blue curve) and 53 GPa initial pressure (black curve). Longitudinal elastic and bulk sound speed curves (using the extrapolation from Zha et al.[18]) are also shown.

In contrast, as shown in Fig. 4, at initial pressures of more than 50 GPa (see Fig. 2b for an example of the raw data), we observe wave speeds consistent with longitudinal elastic compression. Data from samples at initial pressures above 50 GPa are qualitatively similar to shock data[19,21] and different from quasi-isentropic data (as shown, for example, in Fig. 2a). When fit using the shock wave model of ref. 21, these data indicate elastic shock wave speeds which are consistent with longitudinal elastic wave speeds[18] (see

Table 2 of the supplemental information) and inconsistent with the calculated quasi-isentropic compression curve from 53 GPa initial pressure (see Fig. 4), indicating elastic shock compression in this precompression regime. At the piston, similar to previous observations of deformation in thin samples[30,38,39], the elastic wave is very large, and may be expected to be faster than the (low amplitude) longitudinal acoustic wave speed at the initial pressure, consistent with our observation. For comparison to longitudinal acoustic wave speeds, it is reasonable to assume our measured longitudinal wave speed corresponds to an effective stress bounded by the initial and final stress in the sample, as shown in Fig. 4. Acoustic wave speeds have not previously been experimentally measured in deuterium at static compressions greater than 24 GPa. These results also indicate that a sustained longitudinal elastic stress of at least 16 GPa (see Fig. 4 and supplemental information) can be maintained for at least 100 ps (see Fig.2b) in deuterium starting from a static pressure of 55 GPa.

Data at an initial pressure of 36 GPa (shown in the supplemental information) cannot be fit with either a quasi-isentropic model or an elastic shock model, possibly due to kinetics resulting from the relaxation of anisotropic stress on a time scale comparable to the compression time scale (which neither model takes into account). This result suggests that the time scale of material relaxation varies significantly between an initial pressure of ~24 GPa, where relaxation occurs faster than compression, and 51 GPa, where elastic compression does not relax over the ~100 ps duration of our experimental time window.

We speculate that the abrupt deviation in quasi-isentropic data from fits (as shown in Fig. 2a and the supplemental information), typically around 50-80 ps after the wave arrival in the sample, is due to the loss of coherence in the wave front upon the convergence of isobars – the ramp to shock transition[41]. Such a transition was observed in all near 25 GPa initial pressure data, but not observed in data corresponding to initial pressures above 50 GPa. The convergence of isobars in models (for data at near 25 GPa initial pressure) corresponds very well to the timing of the transition in the corresponding deuterium time domain data. Wave interactions upon the convergence of isobars generate reflected and transmitted waves[41] which may reduce the coherence of the wave front, and thus the amplitude of optical reflections from the wave front.

In conclusion, we observe compression wave speeds consistent with quasi-isentropic compression of deuterium over 100 ps to 1.24x initial density from 25 GPa initial pressure. At initial pressures higher than 50 GPa, we observe elastic shocks, indicating that material relaxation has not occurred on the experimental time scale. These results strongly suggest that cryogenic liquid can be quasi-isentropically compressed on an ultrafast time scale, thus providing a route to high density deuterium using orders of magnitude less laser drive energy than required for longer time scale dynamic compression.

Acknowledgements

We acknowledge useful conversations with L. E. Fried, E. J. Reed, B. W. Reed, W. J. Nellis, J. Eggert, G. Collins, R. Smith, M. Howard, B. Militzer, J. Carter, R. Hemley, H.

Radousky, and J. Forbes. This work was performed under the auspices of the U.S. Department of Energy by Lawrence Livermore National Laboratory under Contract No. DE-AC52-07NA27344 with Laboratory directed Research and Development funding (11ERD039), as well as being based on work supported as part of the EFree, an Energy Frontier Research Center funded by the U.S. Department of Energy, Office of Science, Office of Basic Energy Sciences under Grant No. DESC0001057.

References

1. Mao, H. & Hemley, R. J. Ultrahigh-pressure transitions in solid hydrogen. *Rev. Mod. Phys.* **66,** 671–692 (1994).
2. Goncharov, A. F., Hemley, R. J., Mao, H. & Shu, J. New High-Pressure Excitations in Parahydrogen. *Phys. Rev. Lett.* **80,** 101–104 (1998).
3. Tamblyn, I. & Bonev, S. A. Structure and Phase Boundaries of Compressed Liquid Hydrogen. *Phys. Rev. Lett.* **104,** 065702 (2010).
4. Ashcroft, N. W. Hydrogen at high density. *J. Phys. A: Math. Gen.* **36,** 6137–6147 (2003).
5. Lindl, J. Development of the indirect-drive approach to inertial confinement fusion and the target physics basis for ignition and gain. *Phys. Plasmas* **2,** 3933–4024 (1995).
6. Nellis, W. J. Dynamic compression of materials: metallization of fluid hydrogen at high pressures. *Rep. Prog. Phys.* **69,** 1479–1580 (2006).
7. Nellis, W. J. Metallization of fluid hydrogen at 140 GPa (1.4 Mbar): implications for Jupiter. *Planetary and Space Science* **48,** 671–677 (2000).
8. Coppari, F. *et al.* Experimental evidence for a phase transition in magnesium oxide at exoplanet pressures. *Nature Geoscience* **6,** 926–929 (2013).
9. Chen, J. *et al.* Quantum simulation of low-temperature metallic liquid hydrogen. *Nature Communications* **4,** 2064 (2013).
10. Zha, C., Liu, Z., Ahart, M., Boehler, R. & Hemley, R. J. High-Pressure Measurements of Hydrogen Phase IV Using Synchrotron Infrared Spectroscopy. *Physical Review*

Letters **110,** 217402 (5 pp.)–217402 (5 pp.) (2013).

11. Hicks, D. G. *et al.* Laser-driven single shock compression of fluid deuterium from 45 to 220 GPa. *Phys. Rev. B* **79,** 014112 (2009).
12. Bailey, J. E. *et al.* Time-resolved optical spectroscopy measurements of shocked liquid deuterium. *Phys. Rev. B* **78,** 144107 (2008).
13. Wang, J. *et al.* Ramp compression of iron to 273 GPa. *Journal of Applied Physics* **114,** 023513 (2013).
14. 'Slow' compression has been called any of 'quasi-isentropic,' 'ramp,' or 'shockless' compression. Here we use 'quasi-isentropic' to refer to compression by a wave whose speed is given by the bulk sound speed along the thermodynamic isentrope - the conventional definition of sound speed for a material without strength - and we use this term interchangeably with ramp.
15. Smith, R. *et al.* Stiff response of aluminum under ultrafast shockless compression to 110 GPA. *Phys. Rev. Lett.* **98,** 065701 (2007).
16. Jeanloz, R. *et al.* Achieving high-density states through shock-wave loading of precompressed samples. *Proceedings of the National Academy of Sciences* **104,** 9172 –9177 (2007).
17. Armstrong, M. R. *et al.* Prospects for achieving high dynamic compression with low energy. *Appl. Phys. Lett.* **101,** 101904 (2012).
18. Zha, C., Duffy, T. S., Mao, H. & Hemley, R. J. Elasticity of hydrogen to 24 GPa from single-crystal Brillouin scattering and synchrotron x-ray diffraction. *Phys. Rev. B* **48,** 9246–9255 (1993).

19. Armstrong, M. R. *et al.* Ultrafast Shock Initiation of Exothermic Chemistry in Hydrogen Peroxide. *J. Phys. Chem. A* **117,** 13051 (2013).
20. Boehly, T. R. *et al.* Multiple spherically converging shock waves in liquid deuterium. *Phys. Plasmas* **18,** 092706 (2011).
21. Armstrong, M. R., Crowhurst, J. C., Bastea, S. & Zaug, J. M. Ultrafast observation of shocked states in a precompressed material. *J. Appl. Phys.* **108,** 023511 (2010).
22. Benuzzi-Mounaix, A. *et al.* Chirped pulse reflectivity and frequency domain interferometry in laser driven shock experiments. *Phys. Rev. E* **60,** R2488–R2491 (1999).
23. Dlott, D. D. in *Annual Review of Physical Chemistry, Vol 62* (Leone, S. R., Cremer, P. S., Groves, J. T. & Johnson, M. A.) **62,** 575–597 (Annual Reviews, 2011).
24. Evans, R. *et al.* Time- and Space-Resolved Optical Probing of Femtosecond-Laser-Driven Shock Waves in Aluminum. *Phys. Rev. Lett.* **77,** 3359 (1996).
25. Gahagan, K. T., Moore, D. S., Funk, D. J., Reho, J. H. & Rabie, R. L. Ultrafast interferometric microscopy for laser-driven shock wave characterization. *J. Appl. Phys.* **92,** 3679 (2002).
26. Bolme, C. A., McGrane, S. D., Moore, D. S. & Funk, D. J. Single shot measurements of laser driven shock waves using ultrafast dynamic ellipsometry. *J. Appl. Phys.* **102,** 033513 (2007).
27. Pezeril, T. *et al.* Direct Visualization of Laser-Driven Focusing Shock Waves. *Phys. Rev. Lett.* **106,** 214503 (2011).
28. Lin, H.-N., Stoner, R. J., Maris, H. J. & Tauc, J. Phonon attenuation and velocity

measurements in transparent materials by picosecond acoustic interferometry. *Journal of Applied Physics* **69,** 3816–3822 (1991).

29. Mao, H., Xu, J. & Bell, P. Calibration of the Ruby Pressure Gauge to 800-Kbar Under Quasi-Hydrostatic Conditions. *Journal of Geophysical Research-Solid Earth and Planets* **91,** 4673–4676 (1986).
30. Crowhurst, J. C., Armstrong, M. R., Knight, K. B., Zaug, J. M. & Behymer, E. M. Invariance of the Dissipative Action at Ultrahigh Strain Rates Above the Strong Shock Threshold. *Phys. Rev. Lett.* **107,** 144302 (2011).
31. Gladstone, J. H. & Dale, T. P. Researches on the refraction, dispersion and sensitiveness of liquids. *Philos. Trans. R. Soc. London* **153,** 317–343 (1863).
32. Dewaele, A., Eggert, J. H., Loubeyre, P. & Le Toullec, R. Measurement of refractive index and equation of state in dense He, H2, H_{2}O, and Ne under high pressure in a diamond anvil cell. *Phys. Rev. B* **67,** 094112 (2003).
33. Goncharov, A. F., Zaug, J. M., Crowhurst, J. C. & Gregoryanz, E. Optical calibration of pressure sensors for high pressures and temperatures. *Journal of Applied Physics* **97,** 094917 (2005).
34. Reed, B. W., Stolken, J. S., Minich, R. W. & Kumar, M. A unified approach for extracting strength information from nonsimple compression waves. Part I: Thermodynamics and numerical implementation. *J. Appl. Phys.* **110,** 113505 (2011).
35. Zhakhovsky, V. V., Budzevich, M. M., Inogamov, N. A., Oleynik, I. I. & White, C. T. Two-Zone Elastic-Plastic Single Shock Waves in Solids. *Phys. Rev. Lett.* **107,** 135502 (2011).

36. Fowles, R. & Williams, R. Plane stress wave propagation in solids. *J. Appl. Phys.* **41,** 360–363 (1970).

37. Kang, H. S. & Ree, F. H. A variational theory of classical solids. *J. Chem. Phys.* **99,** 2985–2991 (1993).

38. Ashitkov, S. I., Agranat, M. B., Kanel', G. I., Komarov, P. S. & Fortov, V. E. Behavior of aluminum near an ultimate theoretical strength in experiments with femtosecond laser pulses. *JETP Lett.* **92,** 516–520 (2010).

39. Whitley, V. H. *et al*. The elastic-plastic response of aluminum films to ultrafast laser-generated shocks. *J. Appl. Phys.* **109,** 013505 (2011).

40. Aidun, J. & Gupta, Y. Analysis of Lagrangian gauge measurements of simple and nonsimple plane-waves. *J. Appl. Phys.* **69,** 6998–7014 (1991).

41. Fritz, J. N. Overtaking wave interaction, reflected shock or reflected release? *AIP Conf. Proc.* **370,** 271–274 (1996).